Radiationless Decay Mechanism of Cytosine: An Ab Initio Study with Comparisons to the Fluorescent Analogue 5-Methyl-2-pyrimidinone

Kurt A. Kistler and Spiridoula Matsika*

Department of Chemistry, Temple University, Philadelphia, Pennsylvania 19122

Received: September 27, 2006; In Final Form: January 25, 2007

The ultrafast radiationless decay mechanism of photoexcited cytosine has been theoretically supported by exploring the important potential energy surfaces using multireference configuration−interaction ab initio methods for the gas-phase keto-tautomer free base. At vertical excitation, the bright state is S_1 ($\pi\pi^*$) at 5.14 eV, with S_2 ($n_N\pi^*$) and S_3 ($n_O\pi^*$) being dark states at 5.29 and 5.93 eV, respectively. Minimum energy paths connect the Franck−Condon region to a shallow minimum on the $\pi\pi^*$ surface at 4.31 eV. Two different energetically accessible conical intersections with the ground state surface are shown to be connected to this minimum. One pathway involves N^3 distorting out of plane in a sofa conformation, and the other pathway involves a dihedral twist about the C^5-C^6 bond. Each of these pathways from the minimum contains a low barrier of 0.14 eV, easily accessed by low vibronic levels. The path involving the N^3 sofa distortion leads to a conical intersection with the ground state at 4.27 eV. The other pathway leads to an intersection with the ground state at 3.98 eV, lower than the minimum by about 0.3 eV. Comparisons with our previously reported study of the fluorescent cytosine analogue 5-methyl-2-pyrimidinone (5M2P) reveal remarkably similar conformational distortions throughout the decay pathways of both bases. The different photophysical behavior between the two molecules is attributed to energetic differences. Vertical excitation in cytosine occurs at a much higher energy initially, creating more vibrational energy than 5M2P in the Franck−Condon region, and the minimum S_1 energy for 5M2P is too low to access an intersection with the ground state, causing population trapping and fluorescence. Calculations of vertical excitation energies of 5-amino-2-pyrimidinone and 2-pyrimidinone reveal that the higher excitation energy of cytosine is likely due to the presence of the amino group at the 4-position.

1. Introduction

The ability of DNA and RNA to absorb ultraviolet light without significant reaction or fluorescence is a property that is vital for life exposed to sunlight. This property has been given considerable experimental and theoretical attention in recent years,[1] and it has been determined to be largely an intrinsic property of the nucleobases, which display extremely low fluorescent quantum yields and ultra-short excited-state lifetimes in both solution and gas phase, on the order of 1 ps or less. The excited-state lifetime of cytosine, the base of central focus in this study, has been measured at values from 0.72 to 3.2 ps.[2−5] It has been proposed that the DNA/RNA nucleobases, when excited by UV light, rapidly funnel their excited-state population to the ground state through energetically accessible conical intersections (*ci*) between the first excited singlet state, S_1, and the ground state surface, S_0.[1,6−26] Thus, the excited population cannot, in general, remain excited long enough to fluoresce or long enough to be reactive in an intermolecular collision. Instead, the excess energy is rapidly dissipated as vibrational energy (heat) to the surroundings. In order to more easily probe DNA strand conformational dynamics with spectroscopic techniques, a host of fluorescent DNA base analogues[27] have been created, all with structures and functionalities similar to the nucleotides, in order to mimic many of their properties but generally to display much longer fluorescence lifetimes. Theoretical investigations into the structural and electronic differences and similarities between these fluorescent analogues and the nonfluorescent DNA/RNA bases that they mimic could shed considerable light on the molecular properties that contribute to the vital ability of excited DNA/RNA bases to decay radiationlessly after excitation.

We reported a detailed theoretical analysis of the fluorescence mechanism of one of these analogues, the fluorescent cytosine analogue 5-methyl-2-pyrimidinone (5M2P), using multireference configuration−interaction (MRCI) ab initio methods.[28] The structures of both cytosine and 5M2P are shown in Figure 1. 5M2P has a heterocycle ring structure identical to cytosine. It differs from cytosine in that it has a methyl group at the C^5 position and a hydrogen at the C^4 position, whereas cytosine has a hydrogen at the C^5 position and an amino group at the C^4 position. Our interest in 5M2P is its structural and electronic similarities and differences with cytosine, focusing on the energetic and geometric changes involved with its fluorescence behavior. Understanding the photophysical behavior of an excited molecule requires accurate mapping of the potential energy surfaces (PESs), especially the singlet S_1 surface. Kasha's rule[29] states that fluorescence will most likely originate from a population trapped on this surface. Trapping of the S_1 population requires that the *ci* seams between this surface and the ground state surface must be too high in energy compared with the S_1 minimum to be easily accessible or else the S_1 population must be blocked from accessing this *ci* by an energy barrier sufficiently high to bind vibrational levels. In the case of 5M2P, we located two different *ci* seams between the S_1 and the ground

* To whom correspondence should be addressed. E-mail: smatsika@temple.edu.

10.1021/jp0663661 CCC: $37.00
Published on Web 03/17/2007

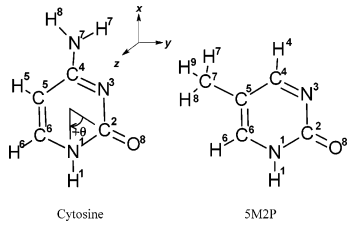

Figure 1. Structures of cytosine and 5M2P with numbering for all geometries presented in this paper. For all geometries presented, cytosine remains approximately parallel to the *xy* plane. The angle θ defines the angle between the *xy* contribution to the static state dipole moment vector and the axis of the C^2-O^8 bond.

state surface, but they were too high in energy so trapping of the S_1 population was shown to be possible; thus, fluorescence for 5M2P was supported theoretically.

We continue this study by presenting the results of MRCI calculations on the photophysical behavior of cytosine. Our goal is to theoretically identify the electronic and structural features needed to facilitate ultrafast radiationless decay of this base and to observe how they differ from 5M2P. While our report on 5M2P was to the best of our knowledge the first such analysis of that base, cytosine has received considerable theoretical attention.[7−14,30] Ismail et al., using complete active space-self consistent field (CASSCF), reported a decay mechanism wherein the bright S_2 $\pi\pi^*$ population undergoes a state switching to the $n_O\pi^*$ surface, with a subsequent accessible channel to the ground state through a gs/$n_O\pi^*$ *ci*.[7] Also located was an energetically blocked gs/$n_N\pi^*$ intersection, with considerable out-of-plane distortion at the intersection by N^3. Merchán and Serrano-Andrés, by using complete active space with second-order perturbation theory (CASPT2) to include dynamical correlation, found S_1 to be $\pi\pi^*$ which crossed with the ground state surface.[8] Other groups have located an accessible S_0/S_1 *ci* with C^5/C^6 diradical character and a commensurate twist around the C^5-C^6 bond. Sobolewski and Domcke located this channel in the cytosine−guanine base pair,[10] and Tomić et al. located a similarly distorted *ci* in isolated cytosine with density functional theory (DFT)/MRCI.[11] Zgierski et al. also recently reported such a decay channel structure for cytosine from results of completely renormalized equation of motion coupled-cluster (CR-EOM-CCSD(T)) calculations of configuration interaction singles (CIS)-optimized geometries.[13] With such a diverse and sometimes conflicting range of proposed mechanisms of the decay of excited cytosine, it is currently unclear which of these is more valid than the others. Indeed, a more accurate picture might actually be a combination of these mechanisms or even other mechanisms entirely. Additionally, some of these previous studies used methods that did not include dynamical correlation for calculating gradients. Dynamical correlation has been shown to be important for predicting the correct order of states and thus is critical when state crossings are involved.[8] In this report, a comprehensive analysis of the pathways for the radiationless decay in cytosine is presented using MRCI methods for both the energies and the gradients, and they are compared with the results reported for the fluorescent analogue 5M2P. Detailed analysis of the differences in photophysical properties of the two molecules requires studies at the same high level of theory.

The methods used to study cytosine will be presented in section 2, including the theoretical treatments and software used. Then, in section 3, results will be discussed, including vertical excitation data, location of stationary points on the singlet-state adiabatic surfaces, *ci*, pathways connecting many of these points, and comparisons with 5M2P. Finally we will conclude and summarize in section 4.

2. Methods

The basis sets for all atoms were the double-ζ plus polarization (cc-pvdz) Gaussian basis sets of Dunning.[31] Cytosine has 58 electrons in total, with 8 heavy atoms (N, O, and C), and 5 hydrogens. All calculations were carried out with no symmetry restrictions. Molecular orbitals (MOs) were obtained from a state-averaged multi-configuration self-consistent field (SA-MCSCF) procedure for the first four singlet states, unless otherwise specified. The five lowest singlet states arise from excitations of π, n_N, and n_O electrons to π^* orbitals, and so the complete active set (CAS) of orbitals was chosen to be 7 π, 1 n_N, and 1 n_O, with a total of 12 electrons in 9 active orbitals. We denote this arrangement as (12, 9). In general, (*n, m*) denotes *n* electrons in *m* active orbitals. The CASSCF calculation generated 2520 reference configurations from this active space, which was used for all subsequent MRCI calculations presented here. The amino nitrogen lone pair was not treated as active in any of the calculations presented in this report.

Three different MRCI expansions were used for calculations. MRCI1 included only single excitation configuration state functions (CSFs) generated from the CAS orbitals, with the core 1s, σ orbitals and one oxygen lone pair remaining always frozen. This low-level expansion contained 637 560 CSFs and was used for single point calculations as well as location and frequency analysis[32] of stationary points and *ci* searches.[33,34] The next expansion, labeled MRCI$\sigma\pi$1, incorporated dynamical correlation of the σ electrons with the π and nonbond electrons. It has been shown[35−39] that dynamical correlation of core and active electrons is important in describing the excited states of organic π systems. Studies on aromatic and planar heteroatom systems that incorporate dynamical correlation with perturbation have supported this assertion, and it has been further shown that inclusion of $\sigma-\pi$ correlation is important when studying the electronic structure and excited states of the nucleobases.[8,19,20,30,40,41] For the MRCI$\sigma\pi$1 expansion, only single excitation CSFs were included in the expansion, but the inclusion of excitations from the 14 σ orbitals and the second oxygen lone pair gave approximately 10 million CSFs. 1s core orbitals were maintained as frozen. This expansion was used to refine MRCI1 single points and for a more accurate optimization of geometries such as important stationary points and *ci*. The third expansion used, labeled MRCI$\sigma\pi$2, includes single excitations from the σ electrons and one oxygen lone pair plus single and double excitations from the CAS orbitals into the virtual orbitals. Double excitations dramatically increase the number of configurations in the expansion, with MRCI$\sigma\pi$2 for this molecule having over 121 million CSFs. MRCI$\sigma\pi$2 was only used for single point calculations of important geometries, and often only the first two states were allowed to converge, since our main focus was on the topology of the S_1 surface.

Linear interpolation (LI) between important geometries was performed in order to quickly give qualitative information about state surface crossings and possible minima and barriers between equilibrated geometries. Calculations presented in this paper did not result in the rotation or translation of cytosine, only distortion, while maintaining the relative orientation as constant. The difference between the Cartesian coordinates of two geometries of interest was calculated, and several geometries were generated by adding this difference times a scaling factor from 0 to 1. This gives the energy profile for a molecular change corresponding to a single concerted motion of all atoms linearly between two geometries. The geometries generated along the LI path can then act as launching points for searches of gradient minima and barriers or can support a connection between

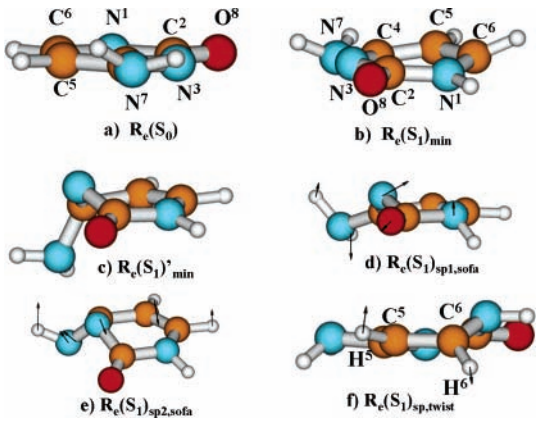

Figure 2. Ground state and S_1 stationary points. The geometries are (a) $\mathbf{R_e}(S_0)$, (b) $\mathbf{R_e}(S_1)_{min}$, (c) $\mathbf{R_e}(S_1)'_{min}$, (d) $\mathbf{R_e}(S_1)_{sp1,sofa}$, (e) $\mathbf{R_e}(S_1)_{sp2,sofa}$, and (f) $\mathbf{R_e}(S_1)_{sp,twist}$, with arrows showing the respective dominant atomic motions on the imaginary vector of each saddle point.

geometries where the gradient is too low to sample effectively in a gradient-directed pathway.

The software used for all calculations was a modified version of the *COLUMBUS Quantum Chemistry Program Suite*, which includes algorithms for locating two- and three-state *ci*.[33,34,42−45] The algorithms use analytic gradients for MRCI wave functions available in *COLUMBUS*.[46] Molecular visualization and graphical rendering was done with Molden.[47]

3. Results and Discussion

3.1. Cytosine. The tautomer used for cytosine is the keto-form free base. The keto-form is likely to be the most stable tautomer in aqueous and physiological environments because of its large dipole.[11] Figure 1 shows the structure of cytosine with the atomic numbering that will be used throughout this paper. Geometries are denoted by **R**. The equilibrium geometry for the singlet state S_m is denoted as $\mathbf{R_e}(S_m)$. Minimum energy points of *ci* seams between states S_I and S_J are denoted as $\mathbf{R_x}$-(*ciIJ*). In section 3.1.1., the ground state and the first three excited singlet states will be characterized on the basis of the results of the three MRCI expansions described in section 2. Vertical excitation energies, along with their calculated oscillator strengths, will be given. Stationary points on the S_1 surface will be presented in section 3.1.2., since this surface seems to be the most important in understanding the photophysical behavior of cytosine. In section 3.1.3., *ci* will be presented, and in section 3.1.4., we will connect points on the S_1 surface with gradient-directed pathways.

3.1.1. Vertical Excitation Energies. The ground state geometry, $\mathbf{R_e}(S_0)$, at the MRCI1 level has C_1 symmetry due to the amino group being pyramidalized and slightly tilted with respect to the ring, which is planar. The tilt of the amino group is such that its lone pair of electrons tilt about 10° toward H^5, and likewise, H^8 on the amino is tilted toward N^3, perhaps from weak electrostatic interactions. The geometry of $\mathbf{R_e}(S_0)$ is shown in Figure 2a. Table 1 presents the vertical excitation energies using MRCI1, MRCI$\sigma\pi$1, and MRCI$\sigma\pi$2 expansions, as well as the energies of all other points presented in this paper. Selected bond lengths and angles for all points are given in Table 2, with a complete table of bond lengths and angles given in Supporting Information (Table SI-1). MRCI$\sigma\pi$1 and MRCI$\sigma\pi$2 energies for the ground state were calculated using the converged geometry obtained at the MRCI1 level. The S_1 state is the bright $\pi\pi^*$ state with an oscillator strength of 0.067. S_2 is a dark $n_N\pi^*$ state with an oscillator strength of 0.002, and S_3 is a dark $n_O\pi^*$ state with an oscillator strength of 0.001. This order of state character is conserved at all three levels of MRCI. Assigning orbital character to each excited state was challenging when using the CAS-MO basis set and the MRCI wave function coefficients, since the nonbonding MOs were quite mixed, and so were the resulting MRCI CSFs. A more absolute assignment was accomplished by analyzing the direction of the static state dipole moments and was also verified by the change in Mulliken charges for N^3 and O^8 compared with the Mulliken charges on these atoms for the S_0 state. Because of the planarity of the ring, the orientation of the static state dipole can be approximated by its in-plane components. The dipole orientation angle is defined in Figure 1. The ground state has a dipole orientation of $\theta = 159.8°$ and a magnitude of 5.90 D. The dipole of the S_1 state has an orientation of $\theta = 141°$, and its magnitude is approximately twice that of S_2 and S_3 (4.33 D, compared with 2.32 D for S_2 and 1.72 D for S_3), showing that the charge on N^3 and O^8 has remained relatively fixed, as expected from a $\pi\pi^*$ character. The state dipole for the S_2 state reflects the loss of N^3 charge with an orientation that is dominated by the carbonyl dipole ($\theta = 177°$, as defined in Figure 1), and thus, S_2 is assigned an $n_N\pi^*$ character. The S_3 state displays a dipole

TABLE 1: S_0 to S_3 Energies at Three Levels of Correlation for Various Geometries of Cytosine[a]

geometry	S_0	S_1	S_2	S_3
		MRCI1 results		
$\mathbf{R_e}(S_0)$	0.000[b]	5.101 $\pi\pi^*$ ($f = 0.067$)[c]	5.394 $n_N\pi^*$ ($f = 0.002$)[c]	5.888 $n_O\pi^*$ ($f = 0.001$)[c]
$\mathbf{R_x}(ci12)'$	0.728	4.638	4.638	5.301
$\mathbf{R_x}(ci12)$	1.687	4.207	4.207	6.122
$\mathbf{R_x}(ci23)$	0.740	4.456	4.847	4.847
$\mathbf{R_e}(S_1)_{min}$	1.519	4.112 (*3.965*)[d]	4.464	5.956
$\mathbf{R_e}(S_1)_{sp1,sofa}$	1.451	4.285 (*4.091*)[d]	5.264	5.468
$\mathbf{R_e}(S_1)_{sp2,sofa}$	2.746	4.235 (*4.116*)[d]	6.295	7.021
$\mathbf{R_e}(S_1)'_{min}$	3.782	4.123 (*4.095*)[d]	6.444	7.222
$\mathbf{R_e}(S_1)_{sp,twist}$	2.241	4.313 (*4.130*)[d]	5.789	6.073
$\mathbf{R_x}(ci01)_{sofa}$	4.133	4.133	6.645	7.382
$\mathbf{R_x}(ci01)_{twist}$	4.186	4.186	7.350	7.644
$\mathbf{R_x}(ci01)'$	4.744	4.744	5.290	8.146
exptl. abs.[e]		4.700	5.333	5.631
exptl. 0−0 origin[f]		3.965		
		MRCI$\sigma\pi$1 results		
$\mathbf{R_e}(S_0)$	0.000[g]	4.941	5.131	5.625
$\mathbf{R_x}(ci12)'$	0.575	4.425	4.531	5.018
$\mathbf{R_x}(ci23)$	0.553	4.353	4.579	4.618
$\mathbf{R_e}(S_1)_{sp1,sofa}$	1.416	4.292	5.153	5.433
$\mathbf{R_e}(S_1)_{sp2,sofa}$	2.708	4.300	6.281	6.281
$\mathbf{R_e}(S_1)_{min}$[h]	1.038	4.035	4.380	5.520
$\mathbf{R_e}(S_1)_{sp,twist}$	2.151	4.362	5.785	6.019
$\mathbf{R_e}(S_1)'_{min}$	3.670	4.331	6.422	7.107
$\mathbf{R_x}(ci01)_{sofa}$[h]	4.406	4.406	6.715	7.294
$\mathbf{R_x}(ci01)_{twist}$[h]	4.260	4.260	7.097	7.416
		MRCI$\sigma\pi$2 results		
$\mathbf{R_e}(S_0)$	0.000[i]	5.136	5.289	5.927
$\mathbf{R_e}(S_1)_{min}$[h]	1.090	4.311(4.164)[d]		
$\mathbf{R_e}(S_1)_{sp1,sofa}$	1.352	4.447(4.303)[d]		
$\mathbf{R_e}(S_1)_{sp2,sofa}$	2.424	4.283(4.164)[d]		
$\mathbf{R_e}(S_1)_{sp,twist}$	2.055	4.459(4.276)[d]		
$\mathbf{R_e}(S_1)'_{min}$	3.376	4.381(4.353)[d]		
$\mathbf{R_x}(ci01)_{sofa}$[h]	4.091	4.446		
$\mathbf{R_x}(ci01)_{twist}$[h]	3.897	4.063		

[a] All values are in electronvolts referenced to the S_0 of the minimized ground state at the MRCI level indicated. [b] MRCI1 S_0 energy for ground state in is −392.775 646 hartree. [c] *f* is the oscillator strength. [d] Italic numbers in parentheses are zero-point energy corrected energies in electronvolts. [e] Žaloudek et al.[49]. [f] Nir et al.[51] [g] MRCI$\sigma\pi$1 S_0 energy for ground state in is −392.911 623 hartree. [h] Indicates geometry was optimized at the MRCI$\sigma\pi$1 level, otherwise the geometry used was optimized at the MRCI1 level. [i] MRCI$\sigma\pi$2 S_0 energy for ground state is −393.034 481 hartree.

TABLE 2: Selected Bond Lengths and Angles for Stationary Points and Conical Intersections[a]

	$\mathbf{R}_e(S_0)$ MRCI1	$\mathbf{R}_e(S_1)_{min}$ MRCI$\sigma\pi$1	$\mathbf{R}_e(S_1)_{sp1,sofa}$ MRCI1	$\mathbf{R}_e(S_1)_{sp2,sofa}$ MRCI1	$\mathbf{R}_e(S_1)'_{min}$ MRCI1	$\mathbf{R}_e(S_1)_{sp,twist}$ MRCI1
N^3-C^2	1.383	1.295	1.336	1.389	1.406	1.321
N^1-C^2	1.403	1.373	1.397	1.397	1.382	1.491
N^1-C^6	1.354	1.398	1.383	1.396	1.390	1.357
C^5-C^6	1.356	1.418	1.424	1.378	1.352	1.476
C^4-N^3	1.298	1.399	1.405	1.403	1.423	1.372
C^4-N^7	1.380	1.402	1.395	1.404	1.413	1.401
C^4-C^5	1.443	1.383	1.370	1.418	1.475	1.377
C^2-O^8	1.195	1.296	1.221	1.192	1.194	1.218
$C^4-N^3-C^2$	120.1	115.9	121.1	120.4	114.3	118.6
$C^6-N^1-C^2$	123.6	118.7	120.3	120.7	121.7	113.9
$N^1-C^2-N^3$	116.4	125.3	115.4	107.0	111.0	119.0
$O^8-C^2-N^3$	123.8	121.4	124.7	128.1	124.4	128.4
$O^8-C^2-N^1$	119.8	113.3	119.5	124.1	124.2	112.6
$C^5-C^6-N^1$	119.7	115.5	119.9	122.4	121.2	111.9
$C^4-C^5-C^6$	116.1	119.4	116.4	116.4	116.1	116.9
$N^7-C^4-N^3$	117.9	114.0	115.1	117.5	114.5	115.0
$C^5-C^4-N^3$	124.1	121.2	116.5	110.3	109.0	122.1
$C^5-C^4-N^7$	118.0	124.7	128.4	126.4	118.5	122.7

	$\mathbf{R}_x(ci12)'$ MRCI1	$\mathbf{R}_x(ci23)$ MRCI1	$\mathbf{R}_x(ci01)_{sofa}$ MRCI$\sigma\pi$1	$\mathbf{R}_x(ci12)$ MRCI1	$\mathbf{R}_x(ci01)_{twist}$ MRCI$\sigma\pi$1	$\mathbf{R}_x(ci01)'$ MRCI1	$\mathbf{R}_x(ci23)$ MRCI1
N^3-C^2	1.345	1.338	1.403	1.278	1.380	1.241	1.338
N^1-C^2	1.390	1.374	1.371	1.358	1.443	1.347	1.374
N^1-C^6	1.388	1.464	1.394	1.403	1.357	1.429	1.464
C^5-C^6	1.423	1.316	1.359	1.424	1.464	1.486	1.316
C^4-N^3	1.397	1.350	1.462	1.401	1.314	1.453	1.350
C^4-N^7	1.394	1.421	1.417	1.397	1.367	1.401	1.421
C^4-C^5	1.367	1.447	1.482	1.369	1.453	1.338	1.447
C^2-O^8	1.215	1.273	1.207	1.326	1.206	1.389	1.273
$C^4-N^3-C^2$	126.4	128.3	111.9	115.5	119.2	111.9	128.3
$C^6-N^1-C^2$	123.2	120.9	120.2	119.1	115.5	114.1	120.9
$N^1-C^2-N^3$	114.7	114.9	112.6	127.2	119.2	131.0	114.9
$O^8-C^2-N^3$	125.2	126.1	121.6	119.6	124.0	122.8	126.1
$O^8-C^2-N^1$	120.1	119.0	125.7	113.2	116.8	105.9	119.0
$C^5-C^6-N^1$	118.6	120.4	120.8	115.0	110.5	111.8	120.4
$C^4-C^5-C^6$	119.4	119.0	117.6	120.0	112.2	118.1	119.0
$N^7-C^4-N^3$	114.9	118.5	113.2	113.1	118.6	111.0	118.5
$C^5-C^4-N^3$	117.6	116.5	106.6	122.2	120.7	120.7	116.5
$C^5-C^4-N^7$	127.4	124.8	117.3	124.4	120.1	127.9	124.8

[a] Bond lengths are in Å, angles are in degrees, and geometries are optimized at the MRCI1 or MRCI$\sigma\pi$1 level, as indicated in the column heading for each geometry.

orientation of $\theta = 119°$, reflecting a loss of charge from the oxygen, and so, this state is assigned an $n_O\pi^*$ character.

The assignment of the $\pi\pi^*$ character to S_1 in cytosine is supported almost universally in the literature by other researchers using a wide variety of theoretical methods such as CIS,[13] CASPT2,[30] quasi-degenerate second-order perturbation theory (QDPT2),[13] DFT/MRCI,[11] and early MRCI utilizing only several thousand CSFs.[48] The assignments of character to the S_2 and S_3 $n\pi^*$ states, however, are not generally consistent, with S_2 being $n_N\pi^*$ and S_3 being $n_O\pi^*$ in some reports and reversed in others. Indeed, the results of our own multi-configuration self consistent field (MCSCF) calculations show S_2 as $n_O\pi^*$ and S_3 as $n_N\pi^*$ when using MOs averaged over four states, but these assignments switch when the MOs are averaged over five states. It is clear, however, that in both of these cases the nonbond orbitals are quite mixed, with an assignment of $n_N\pi^*$ being given to a state that is mostly excitation from N^3 but with a significant, although lesser, amount of excitation from n_O possible as well. MRCI calculations on the ground state geometry using either of these two generated sets of MOs, however, consistently show S_2 to be excitation from the N^3 nonbond and show S_3 as excitation from the O^8 nonbond.

The energies of S_1, S_2, and S_3 at the MRCI1 level are respectively 5.10, 5.39, and 5.89 eV. At the MRCI$\sigma\pi$1 level, these energies are 4.94, 5.13, and 5.63 eV, reflecting a stabilization of about 0.2 eV for each state when $\sigma-\pi$ correlation is included in the wave function. When the highest level of correlation is included at the MRCI$\sigma\pi$2 level, however, the energies destabilize somewhat to 5.14, 5.29, and 5.93 eV, respectively. Experimentally, crystalline cytosine, with corrections to approximate an isolated molecule, gives its maximum absorbance at 37 900 cm^{-1}, or 4.70 eV.[49] This translates into an error of 5.0−8.5% for MRCI. The next two bands, characterized as excitations from nonbond orbitals to the π^*, had low intensity and were observed at 43 000 cm^{-1} and 45 400 cm^{-1}, or 5.33 and 5.63 eV, making the error for MRCI$\sigma\pi$2 0.8% and about 5% for these states, respectively.

3.1.2. S_1 Stationary Points. The S_1 $\pi\pi^*$ surface from vertical excitation leads through a mass-weighted gradient-directed path to a minimum, verified by frequency analysis,[50] at 4.31 eV (MRCI$\sigma\pi$2). The zero-point energy corrected value is 4.16 eV which is 0.2 eV higher than the experimental 0−0 origin.[51] Table 1 gives the first four energy levels for this geometry at the MRCI1 and MRCI$\sigma\pi$1 levels and the first two energies at the MRCI$\sigma\pi$2 level. Bond lengths and bond angles for this point are given in Table 2. This minimum will be called $\mathbf{R}_e(S_1)_{min}$, and it is the global minimum at the MRCI1 and MRCI$\sigma\pi$1 levels. Its structure can be viewed in Figure 2b. The geometry of $\mathbf{R}_e(S_1)_{min}$, compared with the geometry of $\mathbf{R}_e(S_0)$, displays a stretching of the C^2-O^8 bond of about 0.1 Å, as well as a slight

butterfly fold in the ring along the N^1-C^4 axis. The character of this S_1 minimum is primarily $\pi\pi^*$, with a lesser amount of $n_O\pi^*$ mixed in, as is reflected in the stretching of the carbonyl bond. At this geometry, S_2 is 0.3 eV higher than S_1 (MRCI1) and is primarily $n_O\pi^*$ in character with a lesser amount of $\pi\pi^*$ mixed in. S_3 is more than 1.5 eV higher (MRCI1) and is a $n_N\pi^*$ state.

A second verified minimum, labeled $\mathbf{R_e}(S_1)'_{min}$, was also found on the S_1 surface using MRCI1 gradients. Its energy is 4.38 eV at the MRCI$\sigma\pi$2 level. Its first four energies at the MRCI1 and MRCI$\sigma\pi$1 levels and the first two at the MRCI$\sigma\pi$2 level are listed in Table 1, and its geometry can be viewed in Table 2 and Figure 2c. The ring in $\mathbf{R_e}(S_1)'_{min}$ is also distorted out of the planarity of the ground state geometry, but rather than the butterfly fold displayed by $\mathbf{R_e}(S_1)_{min}$, $\mathbf{R_e}(S_1)'_{min}$ is distorted in a "sofa" or "envelope" conformation, with N^3 puckered out of plane and the other five ring atoms remaining largely coplanar. Atom C^4 is strongly pyramidalized, with the other ring atoms remaining relatively unpyramidalized. The character of this S_1 minimum is primarily excitation from the N^3 p_z orbital to the C^4 p_z orbital. If the ring was planar, this character would be assigned as $\pi\pi^*$, but with N^3 being distorted significantly out of plane, this p_z orbital is for the most part decoupled from the π system. Likewise, pyramidalization of C^4 has forced hybridization of its p_z orbital, and it is also decoupled from the π system. Thus, it is probably more accurate to characterize the state at this distorted geometry as an N^3/C^4 diradical. S_2 and S_3 at this geometry are very high in energy, at 6.44 and 7.22 eV, respectively, at the MRCI1 level. These two states are essentially pure $n\pi^*$ in character, and their energetic remoteness from S_1 results in almost no $n\pi^*$ mixing with the S_1 state, as is seen by analysis of the MRCI wave function coefficients.

Three verified first-order saddle points were also located on the S_1 surface at the MRCI1 level. The first four energies of these points at the MRCI1 and MRCI$\sigma\pi$1 levels and the first two energies at the MRCI$\sigma\pi$2 level are presented in Table 1. Two of the three saddle points located at the MRCI1 level display a "sofa" distortion with the N^3 atom distorting out of the plane. Their structures are presented in Figure 2d,e, and bonds and angles are presented in Table 2. The dominant atomic motions on the imaginary vectors of both saddle points are shown with arrows in Figure 2. Both, labeled $\mathbf{R_e}(S_1)_{sp1,sofa}$ and $\mathbf{R_e}(S_1)_{sp2,sofa}$, have geometries intermediate between the two minima $\mathbf{R_e}(S_1)_{min}$ and $\mathbf{R_e}(S_1)'_{min}$, with $\mathbf{R_e}(S_1)_{sp2,sofa}$ having its conformation closer to the "sofa" conformation than the "butterfly" conformation. $\mathbf{R_e}(S_1)_{sp1,sofa}$ is considered the main barrier along the sofa region of S_1, at 4.45 eV at the MRCI$\sigma\pi$2 level, constituting a barrier of 0.14 eV higher than $\mathbf{R_e}(S_1)_{min}$ at this level of dynamical correlation. The imaginary frequency of this saddle point is 502.5i cm^{-1}, and the dominant motion of this vector is that of N^3 distorting in and out of plane. The second S_1 saddle point in this region, $\mathbf{R_e}(S_1)_{sp2,sofa}$, has an imaginary frequency of 198.2i cm^{-1}, and its dominant atomic motions are the amino group moving out of plane, with pyramidalization of C^4, approaching the sofa conformation of $\mathbf{R_e}(S_1)'_{min}$. N^3 remains relatively motionless in this imaginary vector. Its S_1 energy at the MRCI1 level is 4.24 eV, only about 0.12 eV higher than that of $\mathbf{R_e}(S_1)_{min}$ and $\mathbf{R_e}(S_1)'_{min}$, and its character is predominantly $\pi\pi^*$. In section 3.1.4., we will show that these two minima are connected through these two saddle points. At the MRCI$\sigma\pi$2 level, $\mathbf{R_e}(S_1)_{sp2,sofa}$ stabilizes to 4.28 eV, which is actually slightly lower than the S_1 energy of $\mathbf{R_e}(S_1)_{min}$ at this correlation level. This is a consequence of optimizing the geometries at a different level of correlation when the surface is very flat, and thus sensitive to correlation. Like $\mathbf{R_e}(S_1)'_{min}$, the S_2 and S_3 energies at $\mathbf{R_e}(S_1)_{sp2,sofa}$ are above 6 eV, and those states are $n_O\pi^*$ and $n_N\pi^*$, respectively, and are not significantly influencing the character of S_1 in this region.

The third saddle point located on the S_1 surface involves a distortion very different than those described above for $\mathbf{R_e}(S_1)_{sp1,sofa}$ and $\mathbf{R_e}(S_1)_{sp2,sofa}$. $\mathbf{R_e}(S_1)_{sp,twist}$ has an S_1 energy of 4.46 eV at the MRCI$\sigma\pi$2 level. It has an imaginary frequency of 318.9i cm^{-1}. Its conformational distortion is the result of a dihedral twisting of the C^5-C^6 bond, with slight pyramidalization of those atoms. Its imaginary vector, shown in Figure 2e, is dominated by opposite out-of-plane motions of atoms H^5 and H^6 as the C^5-C^6 bond twists, and those two carbons pyramidalize somewhat. Because of this twisting about the C^5-C^6 bond, we label this region of S_1 relative to $\mathbf{R_e}(S_1)_{min}$ the "twist" region.

At the MRCI1 and especially the MRCI$\sigma\pi$1 levels, the energy gap between $\mathbf{R_e}(S_1)'_{sp,twist}$ and the S_1 energy of $\mathbf{R_e}(S_1)_{min}$ is as much as 0.3 eV, but the results of the higher correlation at the MRCI$\sigma\pi$2 level show that the topology of the S_1 surface changes, and this energy barrier decreases. Indeed, when the most dynamical correlation is included in the wave function, the energy of $\mathbf{R_e}(S_1)_{min}$ raises by about 0.2 eV, and the MRCI$\sigma\pi$2 energy of $\mathbf{R_e}(S_1)_{sp,twist}$ is only about 0.15 eV higher than $\mathbf{R_e}(S_1)_{min}$, at 4.46 eV. This is only about a 3.5 kcal/mol barrier and is easily accessible by the S_1 population at $\mathbf{R_e}(S_1)_{min}$, which has excess vibrational energy from vertical excitation.

3.1.3. Conical Intersections. Conical intersections between energy surfaces provide an efficient channel for radiationless transitions and fluorescence quenching. The *ci* of cytosine that are important for its photophysics are presented here. Their energies, as well as the topography of their features, contribute to their role in the behavior of the photoexcited molecule. Other *ci*, less directly involved in the photophysics of cytosine, will also be presented in this section.

The topography of the potential PESs in the vicinity of *ci* can play a significant role in the efficacy of a *ci* to promote a nonadiabatic transition, as has been presented previously.[52−59] For cytosine, which has a 33-dimensional coordinate space, the seam space, where two PESs *I* and *J* are degenerate, is spanned by $33 - 2 = 31$ degrees of freedom, with the remaining two degrees of freedom being the branching coordinates, which lift the degeneracy linearly from the *ci*. These two branching coordinates are the tuning vector and the coupling vector[53] and are denoted as $\mathbf{g}^{IJ}$ and $\mathbf{h}^{IJ}$, respectively, using Yarkony's notation.[52,57] $\mathbf{g}^{IJ}$ is the energy difference gradient, and $\mathbf{h}^{IJ}$ is the gradient of the coupling between states *I* and *J*. They are defined mathematically by

$$\mathbf{g}^{IJ} = \frac{\partial}{\partial \mathbf{R}}[E_I - E_J] \tag{1}$$

$$\mathbf{h}^{IJ} = \left\langle \Psi_I \left| \frac{\partial H}{\partial \mathbf{R}} \right| \Psi_J \right\rangle \tag{2}$$

where E_I and Ψ_I are the energy and eigenfunction of state *I*, respectively. The topography of the *ci* in the branching plane is given in terms of the parameters *g*, *h*, s_x, s_y.[52] The energies of the intersecting states *I* and *J* are then given by

$$E_{I,J}(x,y) = s_x x + s_y y \pm \sqrt{(gx)^2 + (hx)^2} \tag{3}$$

where *x* and *y* are displacements along the $\mathbf{g}^{IJ}$ and $\mathbf{h}^{IJ}$ directions, *g* and *h* are the slopes along those two directions, respectively,

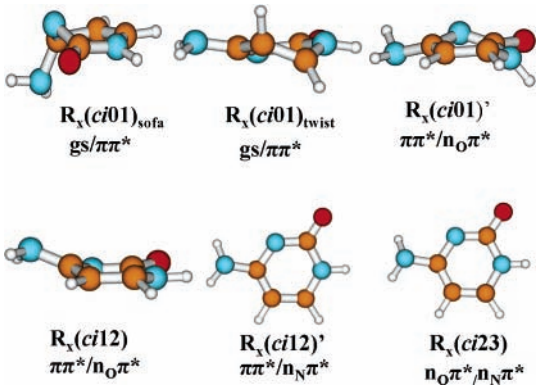

Figure 3. Optimized geometries of *ci* found in cytosine. Geometries shown with top-down views are close to planar C_s symmetry. Those that distort out of plane are shown from the side, oriented to highlight the dominant distortion.

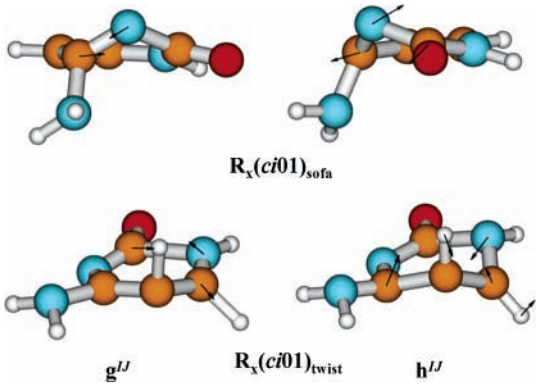

Figure 4. Branching vectors for $\mathbf{R}_x(ci01)_{sofa}$ and $\mathbf{R}_x(ci01)_{twist}$. The $\mathbf{g}^{IJ}$ vectors are shown on the left; the $\mathbf{h}^{IJ}$ vector are shown on the right. Arrows correspond to the dominant motions of atoms on these vectors.

and s_x and s_y give the tilt of the cone. These parameters are used here to characterize the topography of the *ci* found.

Although the points reported in this work are minima on the seam hypersurface, it is not suggested that actual nonadiabatic dynamics occurs only at these points. Indeed, it has been shown that, depending on the accessibility of the seam relevant to the reaction pathways and on the initial wavepacket conditions, extended or narrow ranges of the seam may be important to the dynamics.[60,61] The present study focuses on whether these seams are energetically accessible to enable radiationless decay that will compete with radiative fluorescence. The minimum energy point then serves as the lower bound. If there is not enough energy available to access that point, then there is definitely not enough energy to access the energetically higher regions on the seam. A quantitative discussion that would provide vibrational distributions, rates, and quantum yields would require dynamics and the description of a larger part of the seam. This is beyond the scope of the present work.

3.1.3.1. $\mathbf{R}_x(ci01)_{sofa}$ and $\mathbf{R}_x(ci01)_{twist}$. The ability of cytosine to undergo ultrafast radiationless decay depends on several factors, one of which is the ability of the excited S_1 population to energetically access an intersection with the ground state. Thus, the location of the S_0-S_1 seams is crucial to predicting the photophysical behavior of the molecule. Two such seams, corresponding to the two different kinds of conformational distortion compared with $\mathbf{R}_e(S_1)_{min}$, as described earlier, were located in cytosine. Both have S_0/S_1 minimum energies approximately equal to or lower than the minimum on the S_1 surface, depending on the level of correlation included, and S_0 for each corresponds to the ground state closed-shell PES. The minimum energy points on the *ci* seams are labeled $\mathbf{R}_x(ci01)_{sofa}$ and $\mathbf{R}_x(ci01)_{twist}$. Figure 3 shows their geometries, and Figure 4 shows the branching vectors at these *ci*. Energies are listed in Table 1 for all three levels of correlation, and bond and angle data are listed in Table 2. $\mathbf{R}_x(ci01)_{sofa}$ has a conformation very similar to $\mathbf{R}_e(S_1)'_{min}$ and $\mathbf{R}_e(S_1)_{sp2,sofa}$, with N^3 distorted out of plane in a sofa conformation and strong C^4 pyramidalization. Its energy is 4.10 eV at the MRCI1 level. Optimizing the MRCI1 geometry at the MRCI$\sigma\pi$1 level increases the energy to 4.41 eV, and when higher correlation at the MRCI$\sigma\pi$2 is included, this geometry gives an S_0 energy of 4.09 eV and an S_1 energy of 4.45 eV. The average of these energies is 4.27 eV, which is lower in energy than $\mathbf{R}_e(S_1)_{min}$, $\mathbf{R}_e(S_1)'_{min}$, $\mathbf{R}_e(S_1)_{sp1,sofa}$, or $\mathbf{R}_e(S_1)_{sp2,sofa}$. The highest barrier between this *ci*01 and the $\mathbf{R}_e(S_1)_{min}$ is only 3.5 kcal/mol. Thus, population from vertical excitation should have clear access to this *ci*01, making this *ci* a viable channel for ultrafast radiationless decay of the excited population to the ground state. The character of the S_1 state at this *ci* is virtually the same as that of $\mathbf{R}_e(S_1)'_{min}$, a diradical with excitation primarily from the distorted N^3 p_z orbital (shown in Figure 5c) to the hybridized orbital on the pyramidalized C^4 atom (shown in Figure 5d). The topology of this *ci*01 is shown in Figure 5a, and cone parameters are given in Table 3. It is tilted and relatively symmetric.

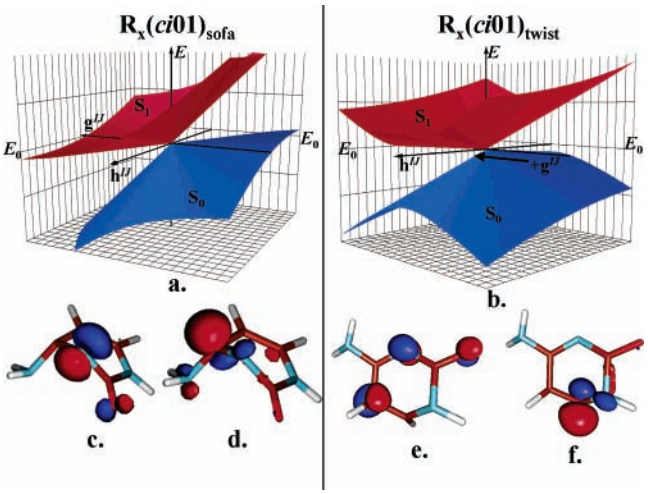

Figure 5. Topographies at $\mathbf{R}_x(ci01)_{sofa}$ and $\mathbf{R}_x(ci01)_{twist}$ and the MOs involved in their S_1 surfaces. (a and b) S_0 and S_1 energies along the branching plane for $\mathbf{R}_x(ci01)_{sofa}$ and $\mathbf{R}_x(ci01)_{twist}$, respectively, are shown, using eq 3 and the cone parameter values for these *ci* given in Table 3. E_0 is the S_0/S_1 energy of the *ci*. (c and d) MOs dominantly excited from and to, respectively, for $\mathbf{R}_x(ci01)_{sofa}$. (e and f) MOs dominantly excited from and to, respectively, for $\mathbf{R}_x(ci01)_{twist}$.

TABLE 3: Cone Parameters, as Defined in Eq 3, for Six Optimized Conical Intersections Found in Cytosine

	s_x	s_y	g	h
$\mathbf{R}_x(ci12)$	−0.0121	−0.0026	0.0403	0.0102
$\mathbf{R}_x(ci12)'$	−0.0337	0.0004	0.1293	0.0248
$\mathbf{R}_x(ci23)$	0.0190	−0.0395	0.0456	0.2079
$\mathbf{R}_x(ci01)_{sofa}$	−0.1113	0.0479	0.1119	0.0896
$\mathbf{R}_x(ci01)_{twist}$	0.0130	−0.2945	0.0224	0.0982
$\mathbf{R}_x(ci01)'$	0.2898	0.0072	0.1391	0.0406

It should be noted here that $\mathbf{R}_x(ci01)_{sofa}$ is conformationally very similar to a *ci*01 found in cytosine by Ismail et al.[7] and also Merchán and Serrano-Andrés.[8] The authors assigned closed-shell/$n_N\pi^*$ character to this *ci*01, but while it was energetically favored compared with the S_1 minimum, CASSCF or CASPT2 gave a substantial barrier on that region of the S_1 surface. MRCI does give a barrier separating $\mathbf{R}_e(S_1)_{min}$ from $\mathbf{R}_x(ci01)_{sofa}$, but it is small.

Another S_0-S_1 seam involving the ground state surface was located in cytosine with MRCI. This *ci*, labeled $\mathbf{R}_x(ci01)_{twist}$, displays conformational distortion primarily as a result of a 114.8° dihedral twist around the C^5-C^6 bond, as well as some pyramidalization of those atoms, with the rest of the ring atoms following this primary distortion. Its character is best described as $\pi\pi^*$, with primary excitation from the p_z orbitals on C^5, N^1, and O^8 to the C^6 p_z orbital, as shown in Figures 5c and 5d. N^1 is somewhat out of plane and is pyramidalized. $\mathbf{R}_x(ci01)_{twist}$ has an S_0/S_1 average energy of 3.98 eV at the MRCI$\sigma\pi$2. Given that the energy at this level of theory for the saddle point separating this *ci*01 from the global MRCI$\sigma\pi$2 minimum is less than 0.20 eV above the minimum, this *ci*01 not only is energetically accessible by a vibrationally excited S_1 population but also is the energetically favored channel to the ground state surface, being about 0.3 eV lower than that of the minimum or $\mathbf{R}_x(ci01)_{sofa}$. The topography for this *ci*, shown in Figure 5b, displays a vertical *ci*, which is the ideal topography for efficient nonadiabatic transitions from an upper to a lower adiabatic surface, in this case S_1 to S_0. Marian et al.[11] and also Zgierski et al.[13] located a similar energetically accessible *ci*01 using DFT/MRCI, also having a C^5-C^6 bond twist, with a reported $H^5-C^5-C^6-H^6$ dihedral angle only about 10° more than our results from MRCI.

Experimentally, it has been shown that cytosine retains its subpicosecond lifetime in a low pH environment.[5] It has been argued[7] that N^3 should be protonated in this case, thus removing a decay channel which includes excitation from N^3, $\mathbf{R}_x(ci01)_{sofa}$ in our study. Then, the relative lack of change in the lifetime for protonated cytidine could indicate that the S_1 pathway to this *ci*01 is blocked by a barrier, implying that this decay channel in unprotonated cytidine is energetically inaccessible. However, in our current study, dynamical correlation energetically favors decay through the lower energy $\mathbf{R}_x(ci01)_{twist}$ which does not involve N^3 excitation and so should not be affected by pH changes regardless of the predicted effect of an acidic environment on the viability of $\mathbf{R}_x(ci01)_{sofa}$ or whether that *ci*01 is blocked by a barrier.

3.1.3.2. Other Conical Intersections. Additional *ci* were located in cytosine. Their energies are below vertical excitation. Although they are not encountered here in a direct mechanism of the S_1 surface deactivation, they could be accessed if the system absorbs higher energy photons, or they may be indirectly involved in the excited-state dynamics of cytosine. Two *ci* seams between the S_1 and the S_2 states were found. Their energies are presented in Table 1; their bond lengths and bond angles are listed in Table 2; the values of the cone parameters presented in eq 3 are listed in Table 3; and the optimized geometries are shown in Figure 3. One of these geometries, labeled $\mathbf{R}_x(ci12)$ at 4.21 eV (MRCI1), is the lowest energy point on a S_1-S_2 seam found for cytosine, and it has $n_O\pi^*/\pi\pi^*$ character which is reflected in a 0.13 Å increase in the C^2-O^8 bond length. This *ci* is close to planar with a slight chairlike conformational distortion, angling C^4 and the amino N^7 above the plane while angling N^1 slightly below the plane. This is clearly seen in the side view shown in Figure 3. Most interesting is the fact that all the bond and angle values of this *ci* are very closely matched with those of $\mathbf{R_e}(S_1)_{min}$, indicating its proximity to that minimum. The second *ci*12, labeled $\mathbf{R}_x(ci12)'$ at 4.64 eV (MRCI1), was located by optimizing the S_1-S_2 crossing seam from vertical excitation. The energies of S_1 and S_2 are very close upon vertical excitation, and thus the S_1-S_2 seam is easily accessed. This *ci* has $n_N\pi^*/\pi\pi^*$ character. The geometry at the minimum energy point on the seam has approximately C_s symmetry, except for the pyramidalized amino nitrogen. Both of these *ci* could serve to funnel higher energy populations onto the $\pi\pi^*$ surface.

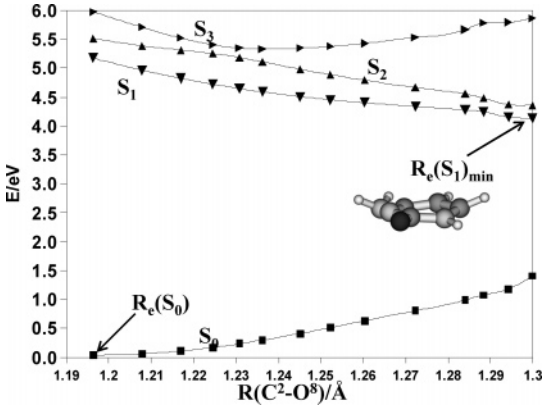

Figure 6. Mass-weighted gradient-driven pathway from vertical excitation, following the MRCI1 gradient of the S_1 state, leading to $\mathbf{R_e}(S_1)_{min}$. Energies in electronvolts of the first four singlet states relative to the minimum of S_0 are plotted as a function of the carbonyl bond length, $R(C^2-O^8)$, in Å.

Two additional *ci* seams were located in cytosine. The MRCI1-optimized geometries are shown in Figure 3; energies are listed in Table 1; and bonds and angles are listed in Table 2. Cone parameters are listed in Table 3. An S_2-S_3 minimum energy *ci* on the $n_N\pi^*/n_O\pi^*$ seam was found at 4.84 eV (MRCI1, Table 1). This *ci* is named $\mathbf{R}_x(ci23)$. The geometry is planar, although the amino N^7 is pyramidalized. The crossing of the $n_N\pi^*$ and $n_O\pi^*$ states changes the character of the S_2 state, and thus the change in the mixing of the character of state S_2 with S_1 is possibly responsible for the barriers located on the S_1 surface. The remaining *ci* located for cytosine is a *ci*01, named $\mathbf{R}_x(ci01)'$ located at 4.74 eV (MRCI1), but it is a stationary point on the $\pi\pi^*/n_O\pi^*$ seam with neither of the states having a closed-shell character. The closed-shell state is at 5.29 eV. The geometry of this *ci* resembles the *ci* found by Merchán and Serrano-Andrés,[8] although the two states in their case were gs/$\pi\pi^*$. Since S_1, S_2, and S_3 are very close in energy, the order of state characters could be very sensitive to the level of correlation used in the calculations.

3.1.4. Pathways. In this section, we will examine how the previously discussed geometries can be connected to enable accessibility to *ci* and efficient radiationless decay. A minimum energy path along the bright $\pi\pi^*$ S_1 state starting from vertical excitation (5.14 eV, MRCI$\sigma\pi$2 level) leads to $\mathbf{R_e}(S_1)_{min}$, as shown in Figure 6, without barriers or state switches. The figure shows the first four MRCI1 energy levels along this pathway. Along this pathway, the S_2 quickly switches character from $n_N\pi^*$ to $n_O\pi^*$, as seen by the crossing between S_2 and S_3, involving the *ci*23 presented in the previous section. The coordinate chosen for this plot is the carbonyl bond stretch which increases as the S_2 $n_O\pi^*$ state stabilizes to an energy close to S_1, thus mixing this character into S_1 somewhat.

Figure 7 shows the accessibility of the two gs/$\pi\pi^*$ *ci* presented in the previous section, $\mathbf{R}_x(ci01)_{sofa}$ and $\mathbf{R}_x(ci01)_{twist}$, from $\mathbf{R_e}(S_1)_{min}$. $\mathbf{R_e}(S_1)_{min}$ is connected to the two saddle points, $\mathbf{R_e}(S_1)_{sp1,sofa}$ and $\mathbf{R_e}(S_1)_{sp,twist}$, corresponding to two different conformational changes. The figure shows these two conformational change directions, "twist" and "sofa", from $\mathbf{R_e}(S_1)_{min}$ on the S_1 surface, along with the rest of the first five energy levels calculated at the MRCI1 level. The figure is several combined energy plots between optimized geometries described in previous sections. The vertical lines correspond to these optimized geometries, shown under the plot, which are con-

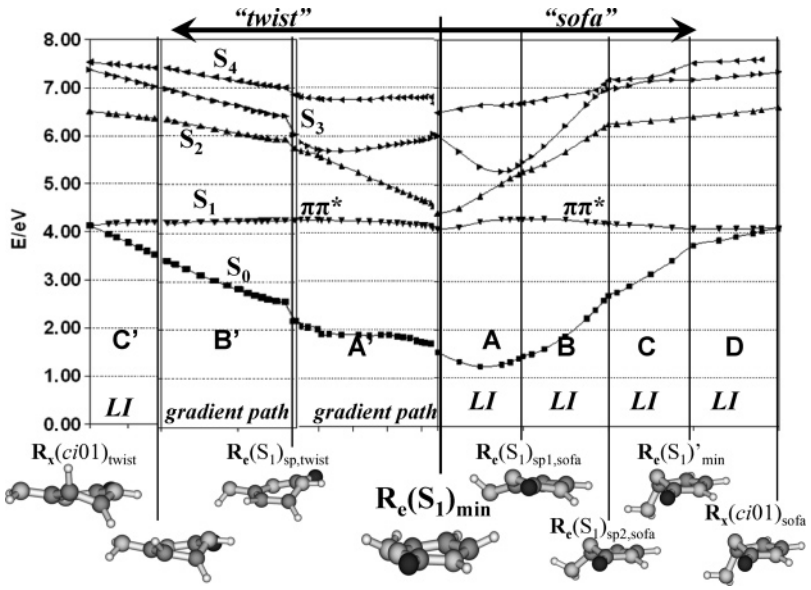

Figure 7. Two directions of conformational distortion along the minimum energy pathway of S_1 cytosine from $\mathbf{R_e}(S_1)_{min}$. The first five singlet state energies at the MRCI1 level are shown for the photophysically important S_1 points with pathway regions connecting them, with structures shown below. Units of energy are electronvolts with respect to the minimum ground state energy. Regions A through D correspond to paths through optimized geometries along the "sofa" distortion direction, as described in the text. Regions A′ through C′ correspond to paths through optimized geometries along the "twist" distortion direction. "LI" means the path was calculated with LI. The coordinates for the two gradient paths are described in the text.

nected within each region. The energies for $\mathbf{R_e}(S_1)_{min}$ are shown in the center of the plot with energy pathways along the sofa direction to the right (regions A−D) and in the twist direction to the left (regions A′−C′).

In the sofa direction, $\mathbf{R_e}(S_1)_{min}$ is connected to the *ci* through two saddle points and a second minimum. Region A shows N^3 distorting out of plane in a sofa fashion to $\mathbf{R_e}(S_1)_{sp1,sofa}$. The S_1 region around this saddle point is too flat to effectively sample via the gradient, but LI shows no additional barriers or minima on the S_1 surface in region A. S_2 here is $n_O\pi^*$ and is rising in energy. This is reflected in the carbonyl compressing from the minimum to $\mathbf{R_e}(S_1)_{sp1,sofa}$. S_3 is $n_N\pi^*$ in this region and is falling in energy. S_4 is a second $n_O\pi^*$ state. In region B from $\mathbf{R_e}(S_1)_{sp1,sofa}$ to $\mathbf{R_e}(S_1)_{sp2,sofa}$, the amino is going more out of plane with the ring, and C^4 is starting to pyramidalize at $\mathbf{R_e}(S_1)_{sp2,sofa}$. This region is also very flat, and so LI was used to connect these two saddle points, showing no additional features between them. An avoided crossing can be seen at the geometry of $\mathbf{R_e}(S_1)_{sp1,sofa}$ between S_2 and S_3, resulting from the S_2/S_3 *ci* described earlier. Further pyramidalizing C^4 in this way leads to $\mathbf{R_e}(S_1)'_{min}$ (region C) with the S_1 character primarily an N^3/C^4 diradical. S_2 to S_4 in this region are rising steeply to greater than 6 eV, resulting in little mixing of the nonbond character into the S_1 state from $\mathbf{R_e}(S_1)'_{min}$ and onward in this direction. Further distortion in the same fashion (region D) eventually leads to the sofa $\mathbf{R_x}(ci01)_{sofa}$ *ci*. This region was also sampled with LI. The character of $\mathbf{R_e}(S_1)'_{min}$ and $\mathbf{R_x}(ci01)_{sofa}$ are both described as N^3/C^4 diradicals.

The pathways connecting $\mathbf{R_e}(S_1)_{min}$ to $\mathbf{R_x}(ci01)_{twist}$ are presented in Figure 7 to the left of $\mathbf{R_e}(S_1)_{min}$, in regions A′−C′. The distortion in this direction is that of a twisting about the C^5-C^6 bond, and this motion of atoms leads to the saddle point $\mathbf{R_e}(S_1)_{sp,twist}$ (region A′), where the imaginary vector is precisely this C^5-C^6 twisting. The plot in this region is a mass-weighted gradient-directed pathway from the saddle point $\mathbf{R_e}(S_1)_{sp,twist}$ to $\mathbf{R_e}(S_1)_{min}$. S_2 in this region is $n_O\pi^*$, which is rising as the system evolves from $\mathbf{R_e}(S_1)_{min}$ toward $\mathbf{R_e}(S_1)_{sp,twist}$. Commensurately, the carbonyl bond is compressing in this direction, from 1.30 Å at $\mathbf{R_e}(S_1)_{min}$ to 1.22 Å at the saddle point. S_3 in region A′ is $n_N\pi^*$ mixed with $\pi\pi^*$, which crosses S_2 near the geometry of the S_1 saddle point. S_4 is a second $\pi\pi^*$ state in this region. Further twisting of the C^5-C^6 bond (region B′) leads from the barrier downhill to a very flat region of S_1, where the gradient is almost zero, to an intermediate geometry, shown at the border of regions B′ and C′. Attempts to locate a stationary point here were unsuccessful, as the system tends to go toward the S_0-S_1 seam with the routine we use for this purpose, and indeed linearly interpolating from this geometry to the twist $\mathbf{R_x}(ci01)_{twist}$ (region C′) gives an essentially flat but slightly downhill path to the *ci*01. In regions B′ and C′, S_2 to S_4 are all mixed character of $n_O\pi^*$, $n_N\pi^*$, and $\pi\pi^*$, and all three are around 6 eV or higher and not significantly influencing the character of S_1, which is $\pi\pi^*$ and quite delocalized throughout the entire path from $\mathbf{R_e}(S_1)_{min}$ to $\mathbf{R_x}(ci01)_{twist}$. At the *ci*, the $H^5-C^5-C^6-H^6$ dihedral angle has increased to 114.8°, and N^1 is somewhat out of plane and pyramidalized. Similar to the energies in the sofa region, energies calculated at the MRCI$\sigma\pi$2 level for geometries in the twist region give the barrier at $\mathbf{R_e}(S_1)_{sp,twist}$ as only about 0.15 eV higher than the minimum on the S_1 surface and so is not considered large enough to impede the highly vibrationally excited S_1 population from reaching $\mathbf{R_x}(ci01)_{twist}$. Furthermore, a small barrier is consistent with the experimental observations of a break-off of the resonance-enhanced multiphoton ionization (REMPI) spectrum close to the 0−0 origin.[51] Significantly, as was previously mentioned, the MRCI$\sigma\pi$2 energy of this *ci*01 is about 0.3 eV lower than the global MRCI$\sigma\pi$2 minimum, further supporting this *ci* as the energetically favored channel for radiationless decay of photoexcited cytosine. Gradient directed paths on S_0 from both $\mathbf{R_x}(ci01)_{sofa}$ and $\mathbf{R_x}(ci01)_{twist}$ lead to the equilibrium ground state geometry.

3.2. Comparisons between Cytosine and 5M2P. We reported a detailed ab initio analysis of the fluorescence mechanism of 5M2P, a fluorescent cytosine analogue, the structure of which is shown in Figure 1.[28] Our interest in this DNA base analogue is in the differences and similarities 5M2P has compared to cytosine. In this section, we will discuss many

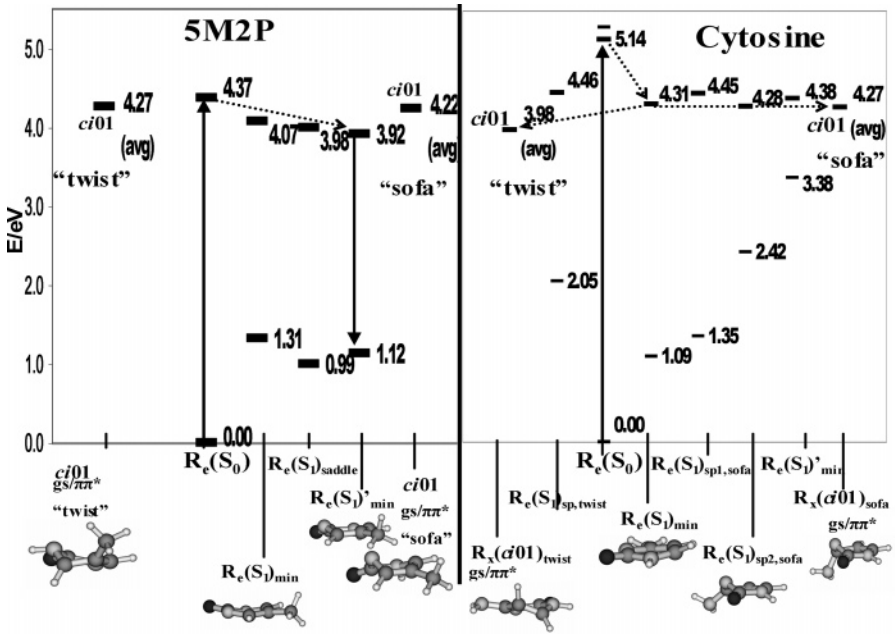

Figure 8. MRCI$\sigma\pi$2 results for 5M2P and cytosine. The important energies of geometries involved in the fluorescence mechanism of 5M2P (left panel) and the ultrafast relaxation mechanism of cytosine (right panel) are shown at the MRCI$\sigma\pi$2 level in units of electronvolts with respect to the minimum of the ground state at each level. 5M2P results are taken from Kistler and Matsika.[28]

of the structural and electronic similarities and differences between these two bases.

Figure 8 shows the MRCI$\sigma\pi$2 results from that previous study on 5M2P, along with results for cytosine at the same level of theory. Energetically, it can be seen that the initial vertical excitation for cytosine is 5.14 eV, while for 5M2P it is only 4.37 eV, lower by about 0.8 eV. The S_1 energies away from the Franck−Condon region are comparable energetically for the two bases, with the S_1 surface for cytosine on average about 0.2 eV higher than the S_1 surface for 5M2P. Therefore, initial excitation creates more excess vibrational energy in cytosine than in 5M2P. In 5M2P, there exists a low-energy minimum, at 3.92 eV, which is below the energetically lowest *ci*01 by about 0.3 eV, low enough to bind vibrational states and eventually fluoresce. In cytosine, this portion of the S_1 surface, toward the $\mathbf{R}_x(ci01)_{sofa}$, contains a small barrier but is essentially flat all the way to the *ci*, so this, by contrast, constitutes a viable radiationless decay channel. Cytosine has a second low-energy decay channel to the ground state as well, the twist *ci*01, while the geometrically similar twist *ci*01 for 5M2P is about 0.4 eV above the global minimum on the S_1 surface. Thus, excluding any structural comparisons, MRCI supports efficient radiationless decay in cytosine but not in 5M2P, on the basis of these energy differences.

Interestingly, the S_0 energy in the sofa region differs significantly for the two bases, with that of 5M2P remaining about 3 eV below the S_1 energy for the region from $\mathbf{R}_e(S_1)_{min}$ to $\mathbf{R}_e(S_1)'_{min}$ and only then rising steeply to meet S_1 at the sofa *ci*01. By contrast, S_0 for cytosine rises continually in its sofa region, and it is only about 1 eV lower than S_1 at $\mathbf{R}_e(S_1)'_{min}$. It can be argued that for cytosine S_0 intersects with S_1 earlier along the minimum energy path on the S_1 surface, crossing at a geometry more similar to that of $\mathbf{R}_e(S_1)'_{min}$.

Conformational similarities between these two bases on excited-state surfaces began to reveal themselves when stationary points on the S_1 surface of cytosine were being calculated. Both molecules are planar in the ground state, and both excite to their bright state and then evolve easily to a local minimum on the S_1 $\pi\pi^*$ surface. The distortion that takes place to reach this minimum for each molecule is very closely matched, both in bond and angle values, as well as the butterfly fold of the ring out of planarity. Overlaid plots of bond and angle values of the two bases are included in Supporting Information (Figure SI-1) for the geometries discussed in this paper and those reported previously for 5M2P. These plots illustrate that both bases display strikingly identical geometries on the excited-state surfaces, including S_1-S_2 intersections, S_2-S_3 intersections, and the MRCI1 S_1 minimum. Indeed, it is clear from these two studies that these two bases have almost identical conformations, on both bright and dark surfaces, along pathways from vertical excitation on down to $\mathbf{R}_e(S_1)_{min}$. Both bases fold along the C^4-N^1 axis in a butterfly fashion, although 5M2P folds by several degrees more than cytosine. Features of the S_1 surface after this butterfly minimum, although structurally very similar, are just different enough to make up what appear to be the dominant differences that ultimately separate the photophysical behavior of these two bases. Both, at the MRCI1 level, have a barrier on the S_1 surface where the sofa-type distortion begins, with N^3 predominantly leaving coplanarity with the other five ring atoms, and beyond this barrier, both bases have a second local minimum where the sofa distortion is more pronounced, $\mathbf{R}_e(S_1)'_{min}$. It is at the barrier that the two bases start to show differences in their bond and angle values. Beyond this second minimum, 5M2P must distort much further to reach the geometry of the *ci*01, whereas the difference in geometry in cytosine between the second minimum and the *ci*01 is much smaller. Electronically, the two molecules display somewhat different character at this *ci*01. Cytosine displays strong diradical character at C^4 and N^3, while 5M2P displays more delocalized $\pi\pi^*$ character. This is reflected in the N^3-C^4 bond lengths for the two bases in this region, with that of 5M2P shorter and more double bond in character than that of cytosine, which stretches from 1.423 to 1.462 Å in the region from $\mathbf{R}_e(S_1)'_{min}$ to the sofa *ci*01. This is likely due to π donation from the amino group, which maintains a distance from C^4 shorter than a C−N single bond throughout this region. The greater π overlap in 5M2P translates into a larger highest occupied molecular orbital−lowest unoccupied molecular orbital (HOMO−LUMO) gap, thus, increasing

the energy of the S_1 surface and the gap between S_0 and S_1 in this region. Similarly, the N^3-C^4 bond stretching seen in cytosine in this region could also explain the higher energy of S_0 compared with that of 5M2P and could contribute to the smaller energy gap.

Twisting about the C^5-C^6 bond for both molecules can eventually lead to the twist *ci*01 intersection with the ground state. However, in the case of 5M2P, this *ci* geometry is too high in energy to be a viable decay channel, and the atoms C^5 and C^6 are somewhat less pyramidalized than those in cytosine. The MOs involved with the S_1 character of both the cytosine and the 5M2P twist *ci*01 are similarly delocalized. A saddle point analogous to cytosine's $\mathbf{R_e}(S_1)_{sp,twist}$ was located in the twist region of 5M2P, with an almost identical distortion to that of cytosine. Bond lengths and bond angles for the ring atoms are compared in a plot in Figure SI-1. The MRCI1 energies for this 5M2P saddle point are $S_0 = 1.67$ eV, $S_1 = 3.86$ ($\pi\pi^*$), 5.26 ($n_N\pi^*$), and 5.85 eV ($n_O\pi^*$), with an S_0/S_1 gap of about 2.2 eV. At the same level of theory, the gap between S_0 and S_1 energies for $\mathbf{R_e}(S_1)_{sp,twist}$ is 2.1 eV or 0.1 eV less than that of 5M2P. Perhaps more important is the fact that for 5M2P the twist *ci*01 is about 0.3 eV higher than this saddle point, while for cytosine the *ci* is lower in energy than the saddle point at all levels of theory. Thus, like the sofa region, 5M2P must destabilize energetically in order to reach degeneracy between S_0 and S_1, while cytosine actually stabilizes. Further investigations into the reasons why the two bases display dramatically different energies at this *ci* are currently in progress.

The initial higher excitation energy of cytosine compared with that of 5M2P is likely to be an important factor in the different photophysical decay mechanisms of these two bases. To probe the reason behind this higher initial excitation, two additional bases were studied at the MRCI1 level: 2-pyrimidinone (2P) and 5-amino-2-pyrimidinone (5A2P). Vertical excitation energies for the optimized ground state structure of 2P were almost matched with 5M2P at 4.65 ($n_N\pi^*$), 4.69 ($\pi\pi^*$), and 5.38 eV ($n_O\pi^*$), with the same ordering of states. Thus, the methyl on 5M2P has almost no role in the energies or character of its excited states. The results of 2P also imply that the amino group on cytosine is necessary for its higher vertical energies. However, when the amino group is moved to the 5-position in 5A2P, the vertical excitation energies are also almost matched with 5M2P, including ordering of the states, at 4.62, 4.66, and 5.33 eV, showing that the amino has almost no effect at C^5. This indicates a $\pi-$resonance interaction of the amino group in cytosine with the ring, which is supported by two important geometrical differences between the ground state structures of cytosine and 5A2P: in cytosine, the amino group is oriented so that its lone pair is almost perpendicular to the ring plane, and the C^4-N^7 bond is 1.38 Å, shorter than the average C−N single bond (about 1.47 Å); in ground state 5A2P, the amino group is rotated about 90° to the ring, and the C^5-N^7 bond length is 1.42 Å. This shows that the amino group in 5A2P is essentially decoupled from the ring π system and is not included in the overall π resonance of the ring. Thus, we propose that the presence and position of the amino group on the ring is critical to the higher excitation energy of cytosine, and it is largely due to π donation from the amino nitrogen lone pair into the ring. Further investigations into the details of the role of the amino group in the photophysics of cytosine are currently in progress.

Besides the energetic arguments detailed above, a comparison of the photophysical behaviors of cytosine and 5M2P will benefit from an analysis of the nonadiabatic coupling[33,52,62,63] between S_1 and S_0 for each base at geometries close to each of the two S_0-S_1 seams presented in this study: sofa and twist. The nonadiabatic coupling vector **f** for transitions between two adiabatic PESs *I* and *J* is defined in eq 4:

$$\mathbf{f}^{JI} = \left\langle \Psi_J \left| \frac{\partial \Psi_I}{\partial \mathbf{R}} \right\rangle = \frac{1}{E_I - E_J} \left\langle C^J \left| \frac{\partial H}{\partial \mathbf{R}} \right| C^I \right\rangle + \sum_{i,j} D_{i,j}^{JI} \left\langle \phi_i \left| \frac{\partial \phi_j}{\partial \mathbf{R}} \right\rangle \right. \right. \quad (4)$$

where $\Psi_I = \sum_i C_i^I \phi_i$ is the MRCI expansion for state *I* in the basis of CSFs ϕ_i, and $D_{i,j}^{JI}$ is the transition density matrix between state *J* and state *I*. By calculating the magnitude of **f** for geometries on the S_1 surface close to $\mathbf{R_x}(ci01)_{sofa}$ and $\mathbf{R_x}(ci01)_{twist}$ for both cytosine and 5M2P, a qualitative comparison of the probabilities of nonadiabatic transitions from S_1 to S_0 can be made for the two bases in these two regions of S_1.

Following the MRCI method[33,59] and given the conformational similarities the two bases exhibit for S_1 geometries discussed in this study, the magnitude of **f**, |**f**|, was calculated for geometries in two regions for each base: points linearly interpolated between $\mathbf{R_e}(S_1)'_{min}$ and $\mathbf{R_x}(ci01)_{sofa}$ and also points linearly interpolated between $\mathbf{R_e}(S_1)_{sp,twist}$ and $\mathbf{R_x}(ci01)_{twist}$. Figure 9 shows plots of |**f**| in $bohr^{-1}$ as a function of the N^3-C^4 bond length, $\mathbf{R}(N^3-C^4)$, for the sofa region and shows |**f**| as a function of the $X-C^5-C^6-H^6$ dihedral angle in the twist region (where X = H for cytosine and X = CH_3 for 5M2P). It can be seen that in the twist region (regions C′ and D′, Figure 7) the values for |**f**| for the two bases follow almost identical trends and magnitudes from the saddle point to the vicinity of the twist *ci*01 (|**f**| at the intersection itself is infinity, but the value for the dihedral angle at the twist *ci*01 for each base is given on the *x* axis for reference). This implies that the nonadiabatic transition probabilities close to the twist *ci*01 for each base are about equal, and so the energetic accessibility differences at the twist *ci*01 for the two bases are likely to be the dominant factor in how the S_1 population of each base behaves in this region of S_1. In the sofa region (region D, Figure 7), however, cytosine displays about a factor of 10 more coupling compared with the same region in 5M2P, even for geometries very close to the sofa *ci*01. The reason for this is that in the sofa region of cytosine the S_0 PES is much higher than in 5M2P, making the gap between S_1 and S_0 much smaller in cytosine, as discussed above. Since the first term of the right-hand side of eq 4 is the dominant term, **f** varies almost linearly with the inverse of ΔE_{01}, and so this smaller energy gap in cytosine dramatically increases |**f**| in this region compared with the energy gap in 5M2P. Thus, both the S_1 energetic differences and the resulting coupling differences are important contributions in this region for the photophysical behavior differences between cytosine and 5M2P.

The large derivative coupling in this region of cytosine generates higher nonadiabatic transition rates and indicates that the sofa *ci*01 seam extends close to the minimum energy pathway for cytosine in the sofa region. It has been shown before that the position of the *ci* seam relative to the minimum energy pathway can have an effect on the nonadiabatic dynamics producing radiationless transitions either in an extended region of the seam or just close to the minimum energy point.[60,61]

4. Conclusions and Summary

The ultrafast radiationless decay of photoexcited cytosine has been supported theoretically with the MRCI calculations presented in this paper. Initial absorption of a UV photon excites the ground state system to S_1, the bright $\pi\pi^*$ state at 5.14 eV.

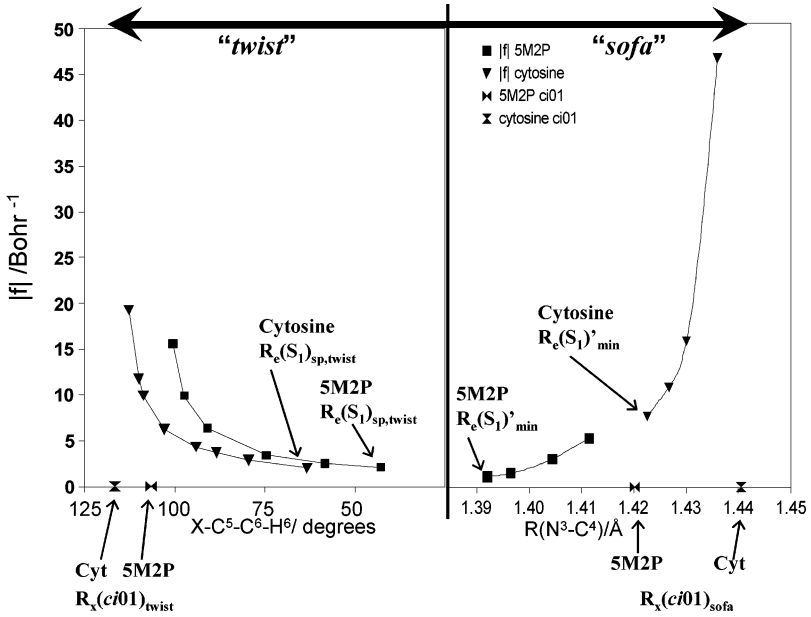

Figure 9. Magnitude of the nonadiabatic coupling vector **f** for regions close to $\mathbf{R}_x(ci01)_{twist}$ and $\mathbf{R}_x(ci01)_{sofa}$ for cytosine and 5M2P. Triangles correspond to cytosine points, and squares correspond to 5M2P points. The left panel shows $|\mathbf{f}|$ in $Bohr^{-1}$ as a function of the X—C^5—C^6—H^6 dihedral angle, in degrees, where X═H for cytosine and X═CH_3 for 5M2P, corresponding to the S_1 path for each base from $\mathbf{R}_e(S_1)_{sp,twist}$ to $\mathbf{R}_x(ci01)_{twist}$ (region B′ and C′ in Figure 7). The values of this dihedral angle for $\mathbf{R}_x(ci01)_{twist}$ for each base are shown as symbols on the *x* axis. The right panel shows $|\mathbf{f}|$ in $Bohr^{-1}$ as a function of the N^3—C^4 bond length for each base in the S_1 path from $\mathbf{R}_e(S_1)'_{min}$ to $\mathbf{R}_x(ci01)_{sofa}$ (region D in Figure 7). The values of this bond length for $\mathbf{R}_x(ci01)_{twist}$ for each base are shown as symbols on the *x* axis.

The S_1 surface has a minimum at 4.31 eV which exhibits stretching of the carbonyl by about 0.1 Å and exhibits folding of the ring slightly in a butterfly fashion along the N^1/C^4 axis. Two *ci* seams have been located which are connected to the S_1 minimum through barriers of about 0.15 eV. Pathways connecting the S_1 minimum to the sofa *ci*01 seam show a lower second barrier and a second minimum. At this geometry, the system is described best as an N^3/C^4 diradical on the $\pi\pi^*$ surface. The *ci* between S_1 and the closed-shell S_0 surface has a geometry almost identical to the minimum and energy of 4.27 eV. Excess vibrational energy of the S_1 population from vertical excitation, about 0.8 eV above the global minimum, assures that the population can efficiently reach this *ci*01, making this *ci* an effective channel for ultrafast decay to the ground state. The S_1 minimum at 4.31 eV, is also connected to a second *ci*01 seam. In this second pathway, the so-called twist direction, cytosine twists dihedrally about its C^5—C^6 bond, creating considerable ring distortion out of plane. This pathway, like the sofa direction, has a low barrier of 0.15 eV, compared with the global minimum. Twisting motion of the C^5—C^6 bond leads to a second *ci* with the ground state, lower in energy compared with the *ci* located in the sofa region of S_1. This *ci* has an energy of 3.98 eV, which is about 0.3 eV lower than the global minimum or the sofa *ci*01, making this the more energetically favored *ci*01. Thus, we have shown that cytosine has two viable channels for ultrafast radiationless decay of its photoexcited state to the ground state surface. Experimentally bi-exponential decay signals, by time-resolved photoelectron spectra and femtosecond multiphoton ionization, support the idea of more than one decay channel.[64,65]

Results of cytosine were compared with our previously published results of its fluorescent analogue, 5M2P. Comparisons of the important bonds and angles of these two bases revealed striking matches in the geometrical distortions along virtually all excited-state surfaces. As well, in 5M2P, the S_1 system was shown to be connected to both a sofa- and twist-distorted *ci*01, with geometrical similarity compared to cytosine especially matched in the twist *ci*01 region. However, 5M2P is excited only to about 4.4 eV, leading to less excess vibrational energy in the S_1 population, while cytosine is excited initially to 5.14 eV, leading to a more vibrationally excited S_1 population. 5M2P was also shown to stabilize to an S_1 minimum at least 0.3 eV below the energies of the two located *ci* with the ground state surface, thus trapping the S_1 population and enabling fluorescence from the longer-lived S_1 population. Comparing the calculated vertical excitation energies for 5M2P and cytosine to those for 2-pyrimidinone revealed that the 5-methyl has at most minimal electronic effect on the vertical excitation energies of 5M2P and revealed that the lack of the 4-amino group seems to be the source of the major differences in the photophysics of 5M2P and cytosine. Comparing the excitation energy of cytosine to the vertical excitation energies and geometry of ground state 5-amino-2-pyrimidinone, which displayed energies very close to those of 5M2P, indicates that the initial higher excitation energy of cytosine is likely due to resonance of the 4-amino with the ring π system, which is not present when the amino is at C^5. In addition to the role of the amino group as a proton donor in a base pair interaction with guanine, results of this study also implicate its role in the high vertical excitation energy of cytosine, as well as its enhancement of nonadiabatic coupling in the vicinity of one of its S_0/S_1 seams. Both of these effects can promote radiationless decay of photoexcited cytosine. Further investigations into the details of these important structural and electronic factors are currently in progress.

Acknowledgment. This work was supported by the National Science Foundation under Grant CHE-0449853 and Temple University.

Supporting Information Available: A complete table of bond lengths and angles, as well as plots comparing values of bond lengths and angles in cytosine and 5M2P, for all geometries discussed in this study. This material is available free of charge via the Internet at http://pubs.acs.org.

References and Notes

(1) Crespo-Hernandez, C. E.; Cohen, B.; Hare, P. M.; Kohler, B. *Chem. Rev.* **2004**, *104*, 1977.

(2) Pecourt, J.-M. L.; Peon, J.; Kohler, B. *J. Am. Chem. Soc.* **2001**, *123*, 10370.

(3) Peon, J.; Zewail, A. H. *Chem. Phys. Lett.* **2001**, *348*, 255.

(4) Kang, H.; Lee, K. T.; Jung, B.; Ko, Y. J.; Kim, S. K. *J. Am. Chem. Soc.* **2002**, *124*, 12958.

(5) Malone, R. J.; Miller, A. M.; Kohler, B. *Photochem. Photobiol.* **2003**, *77*, 158.

(6) Klessinger, M.; Michl, J. *Excited States and Photochemistry of Organic Molecules;* VCH Publishers, Inc.: Cambridge, U.K., 1995.

(7) Ismail, N.; Blancafort, L.; Olivucci, M.; Kohler, B.; Robb, M. *J. Am. Chem. Soc.* **2002**, *124*, 6818.

(8) Merchán, M.; Serrano-Andrés, L. *J. Am. Chem. Soc.* **2003**, *125*, 8108.

(9) Merchán, M.; Serrano-Andrés, L.; Robb, M.; Blancafort, L. *J. Am. Chem. Soc.* **2005**, *127*, 1820.

(10) Sobolewski, A. L.; Domcke, W. *Phys. Chem. Chem. Phys.* **2004**, *6*, 2763.

(11) Tomić, K.; Jörg, T.; Marian, C. M. *J. Phys. Chem. A* **2005**, *109*, 8410.

(12) Zgierski, M. Z.; Patchkovskii, S.; Fujiwara, T.; Lim, E. C. *J. Phys. Chem A* **2005**, *109*, 9384.

(13) Zgierski, M. Z.; Patchkovskii, S.; Lim, E. C. *J. Chem. Phys.* **2005**, *123*, 081101.

(14) Blancafort, L.; Robb, M. A. *J. Phys. Chem. A* **2004**, *108*, 10609.

(15) Sobolewski, A. L.; Domcke, W. *Eur. Phys. J. D* **2002**, *20*, 369.

(16) Perun, S.; Sobolewski, A. L.; Domcke, W. *J. Am. Chem. Soc.* **2005**, *127*, 6257.

(17) Marian, C. M. *J. Chem. Phys.* **2005**, *122*, 104314.

(18) Chen, H.; Li, S. *J. Phys. Chem. A* **2005**, *109*, 8443.

(19) Matsika, S. *J. Phys. Chem A* **2005**, *109*, 7538.

(20) Matsika, S. *J. Phys. Chem. A* **2004**, *108*, 7584.

(21) Gustavsson, T.; Bányász, Á.; Lazzarotto, E.; Markovitsi, D.; Scalmani, G.; Frisch, M. J.; Barone, V.; Improta, R. *J. Am. Chem. Soc.* **2006**, *128*, 607.

(22) Perun, S.; Sobolewski, A. L.; Domcke, W. *Chem. Phys.* **2005**, *313*, 107.

(23) Nielsen, S. B.; Sølling, T. I. *ChemPhysChem* **2005**, *6*, 1276.

(24) Blancafort, L. *J. Am. Chem. Soc.* **2006**, *128*, 210.

(25) Perun, S.; Sobolewski, A. L.; Domcke, W. *J. Phys. Chem A* **2006**, *110*, 13238.

(26) Serrano-Andrés, L.; Merchán, M.; Borin, A. C. *Proc. Natl. Acad. Sci. U.S.A.* **2006**, *103*, 8691.

(27) Rist, M. J.; Marino, J. P. *Curr. Org. Chem.* **2002**, *6*, 775.

(28) Kistler, K. A.; Matsika, S. *Photochem. Photobiol.* **2007**, in press.

(29) Kasha, M. *Discuss. Faraday Soc.* **1950**, *9*, 14.

(30) Fülscher, M. P.; Roos, B. O. *J. Am. Chem. Soc.* **1995**, *117*, 2089.

(31) Dunning, T. H. *J. Chem. Phys.* **1989**, *90*, 1007.

(32) Császár, P.; Pulay, P. *J. Mol. Struct.* **1984**, *114*, 31.

(33) Lischka, H.; Dallos, M.; Szalay, P. G.; Yarkony, D. R.; Shepard, R. *J. Chem. Phys.* **2004**, *120*, 7322.

(34) Dallos, M.; Lischka, H.; Shepard, R.; Yarkony, D. R.; Szalay, P. G. *J. Chem. Phys.* **2004**, *120*, 7330.

(35) Borden, W. T.; Davidson, E. R. *Acc. Chem. Res.* **1996**, *29*, 67.

(36) Maksić, Z. B.; Barić, D.; Petanjek, I. *J. Phys. Chem. A* **2000**, *104*, 10873.

(37) Jug, K.; Köster, A. M. *J. Am. Chem. Soc.* **1990**, *112*, 6772.

(38) Kuwajima, S.; Soos, Z. G. *J. Am. Chem. Soc.* **1987**, *109*, 107.

(39) Jhigalko, M. V.; Shishkin, O. V.; Gorb, L.; Leszczynski, J. *J. Mol. Struct.* **2004**, *693*, 153.

(40) Lorentzon, J.; Fülscher, M. P.; Roos, B. O. *J. Am. Chem. Soc.* **1995**, *117*, 9265.

(41) Fülscher, M. P.; Serrano-Andrés, L.; Roos, B. O. *J. Am. Chem. Soc.* **1997**, *119*, 6168.

(42) Lischka, H.; Shepard, R.; Brown, F. B.; Shavitt, I. *Int. J. Quantum Chem.* **1981**, *15*, 91.

(43) Lischka, H.; Shepard, R.; Pitzer, R. M.; Shavitt, I.; Dallos, M.; Müller, T.; Szalay, P. G.; Seth, M.; Kedziora, G. S.; Yabushita, S.; Zhang, Z. *Phys. Chem. Chem. Phys.* **2001**, *3*, 664.

(44) Lischka, H.; Shepard, R.; Shavitt, I.; Pitzer, R. M.; Dallos, M.; Müller, T.; Szalay, P. G.; Brown, F. B.; Ahlrichs, R.; Böhm, H. J.; Chang, A.; Comeau, D. C.; Gdanitz, R.; Dachsel, H.; Ehrhardt, C.; Ernzerhof, M.; Höchtl, P.; Irle, S.; Kedziora, G.; Kovar, T.; Parasuk, V.; Pepper, M. J. M.; Scharf, P.; Schiffer, H.; Schindler, M.; Schüler, M.; Seth, M.; Stahlberg, E. A.; Zhao, J.-G.; Yabushita, S.; Zhang, Z. **2001**.

(45) Matsika, S.; Yarkony, D. R. *J. Chem. Phys.* **2002**, *117*, 6907.

(46) Lischka, H.; Dallos, M.; Shepard, R. *Mol. Phys.* **2002**, *100*, 1647.

(47) Schaftenaar, G.; Noordik, J. H. *J. Comput.-Aided Mol. Des.* **2000**, *14*, 123.

(48) Petke, J. D.; Maggiora, G. M.; Christoffersen, R. E. *J. Phys. Chem.* **1992**, *96*, 6992.

(49) Žaloudek, F.; Novros, J. S.; Clark, L. B. *J. Am. Chem. Soc.* **1985**, *107*, 7344.

(50) Pulay, P.; Fogarasi, G.; Pongor, G.; Boggs, J. E.; Vargha, A. *J. Am. Chem. Soc.* **1983**, *105*, 7037.

(51) Nir, E.; Miller, M.; Grace, L. I.; Vries, M. S. D. *Chem. Phys. Lett.* **2002**, *355*, 59.

(52) Yarkony, D. R. *J. Phys. Chem A* **2001**, *105*, 6277.

(53) Atchity, G. J.; Xantheas, S. S.; Ruedenberg, K. *J. Chem. Phys.* **1991**, *95*, 1862.

(54) Ben-Nun, M.; Molnar, F.; Schulten, K.; Martinez, T. J. *Proc. Natl. Acad. Sci. U.S.A.* **2002**, *99*, 1769.

(55) Köppel, H.; Domcke, W.; Cederbaum, L. S. *Adv. Chem. Phys.* **1984**, *57*, 59.

(56) Domcke, W.; Stock, G. *Adv. Chem. Res.* **1997**, *100*, 1.

(57) Yarkony, D. R. *Acc. Chem. Res.* **1998**, *31*, 511.

(58) *Conical Intersections: Electronic Structure, Dynamics & Spectroscopy;* Domcke, W., Yarkony, D. R., Köppel, H., Eds.; World Scientific Publishing Co. Pte., Ltd.: Singapore, 2004; Vol. 15.

(59) Lengsfield, B. H.; Yarkony, D. R. Nonadiabatic Interactions Between Potential Energy Surfaces: Theory and Applications. In *State-Selected and State-to-State Ion-Molecule Reaction Dynamics, Part 2;* Baer, M., Ng, C.-Y., Eds.; John Wiley & Sons, Inc.: New York, 1992; Vol. LXXXII, p 1.

(60) Weingart, O.; Migani, A.; Olivucci, M.; Robb, M. A.; Buss, V.; Hunt, P. *J. Phys. Chem. A* **2004**, *108*, 4685.

(61) Hunt, P. A.; Robb, M. A. *J. Am. Chem. Soc.* **2005**, *127*, 5720.

(62) Billing, G. D.; Baer, M.; Mebel, A. M. *Chem. Phys. Lett.* **2003**, *372*, 1.

(63) Baer, M.; Ve'rtesi, T.; Halász, G. J.; Vibók, Á.; Suhai, S. *Faraday Discuss.* **2004**, *127*, 337.

(64) Ullrich, S.; Schultz, T.; Zgierski, M. Z.; Stolow, A. *Phys. Chem. Chem. Phys.* **2004**, *6*, 2796.

(65) Canuel, C.; Mons, M.; Piuzzi, F.; Tardivel, B.; Dimicoli, I.; Elhanine, M. *J. Chem. Phys.* **2005**, *122*, 0743176.